# Mott insulator polariton in $MoSe_2/WS_2$ moiré lattice

Xichen Guo[1#], Hao Ge[1#], Kenji Watanabe[2], Takashi Taniguchi[3], Zhanghai Chen[4], Jie Gu[1*]

[1]State Key Laboratory of Surface Physics and Department of Physics, Fudan University, Shanghai, China

[2]Research Center for Electronic and Optical Materials, National Institute for Materials Science, 1-1 Namiki, Tsukuba, Japan

[3]Research Center for Materials Nanoarchitectonics, National Institute for Materials Science, 1-1 Namiki, Tsukuba, Japan

[4]Department of Physics, College of Physical Science and Technology, Xiamen University, Xiamen, China

[#]Those authors contribute equally

*Email: gujielog@fudan.edu.cn

## Abstract

Transition metal dichalcogenide moiré superlattices host rich correlated electronic states with high tunability. Their integration with optical cavities offers a new platform to explore hybrid light-matter interactions. However, the interplay between electron correlations and polariton formation remains uncharted. Here, we demonstrate the realization of a Mott insulator polariton in a gate-tunable $MoSe_2/WS_2$ moiré heterostructure embedded in a microcavity at the moiré lattice filling of $v = 1$. A silver top layer was used to gate the moiré lattice and form the cavity reflection layer. Magnetic field studies indicate that the polaritons inherit valley Zeeman splitting from the moiré excitons, exhibiting saturation behavior similar to the bare moiré excitons. Our work establishes moiré polaritons as an electrically and magnetically tunable platform for engineering quantum phases of light and matter.

**Keywords:** TMDs, mott insulator, polariton, electron correlations

Transition metal dichalcogenide (TMD) moiré systems have emerged as a fascinating platform for exploring strongly correlated phenomena due to their unique electronic properties and tunable moiré superlattices[1]. These systems exhibit a rich variety of quantum states, including Mott insulators[2,3], superconductivity[4,5], Wigner crystals[6,7] and others, driven by the strong interactions between electrons confined in the moiré potential. Concurrently, polaritons—hybrid quasiparticles arising from the strong coupling between excitons and cavity photons—have attracted significant attention for their nonlinear optical properties and potential applications in quantum optics[8–10]. The intrinsic nonlinearity of polaritons stems from the excitonic component, which can be further enhanced by engineering the exciton-photon coupling strength or the underlying material properties.

The integration of TMD moiré systems with optical cavity presents a promising avenue for exploring novel quantum phenomena at the intersection of correlated electrons, excitons, and photons. In such a hybrid system, the strong correlations inherent to TMD moiré lattices could influence the behavior of polaritons, potentially leading to enhanced nonlinearities and new collective states. This synergy could also provide a unique platform for studying many-body effects in a highly tunable and optically accessible system.

Despite the exciting potential of integrating TMD moiré systems with polaritons, this hybrid platform remains largely unexplored. Previous studies on moiré polaritons have primarily focused on the coupling between bare moiré excitons and photons in the absence of electron doping[11,12], thus neglecting the critical role of electron correlation effects. However, electron correlations raise several fundamental questions, such as whether polaritons persist under electron correlations—a prerequisite for exploring other polariton phenomena. Additionally, questions concerning how correlated electronic states modulate polariton properties, such as nonlinearities and coupling strengths, remain unknown. In this work, we aim to address the first question by investigating the existence of polaritons under electron correlation and systematically studying their doping dependence.

We start by fabricating a single-gate moiré polariton Device 1, as illustrated in Fig. 1a. The device comprises a top silver mirror and a bottom distributed Bragg reflector (DBR) mirror as the cavity reflecting layers. A $MoSe_2/WS_2$ moiré heterostructure was embedded between thin hexagonal boron nitride (hBN) layers, and the cavity mode was precisely controlled by adjusting the thickness of the poly (methyl methacrylate) (PMMA) layer. Detailed fabrication procedures are provided in the Supplementary S1.

In this geometry, the top silver layer functions not only as an optical mirror but also as an electrical top gate, enabling carrier injection into the moiré layers when voltage is applied. In the two-dimensional (2D) materials community, particularly in TMD polariton research[13–15], graphite gates have been predominantly employed—either in single or dual-gate configurations—to inject carriers into the material. This preference stems from their compatibility with established material fabrication techniques. However, integrating graphite gates into optical cavities introduces significant optical losses due to their inherent absorption, which degrades the cavity quality factor and compromises polariton applications. By utilizing a silver top gate, the gate-induced optical loss can be effectively mitigated.

We also fabricated a bare moiré device (Device 2) using a graphite gate electrode, but not embedded in an optical cavity, as illustrated in Supplementary Fig. S1. This device enables characterization of the optical response of the moiré superlattice as a function of electron doping. Device 1 is not suitable for this measurement because its final silver deposition integrates the heterostructure into the cavity, leaving only cavity optical modes accessible; the bare moiré lattice optical response cannot be accessed.

We present the doping dependent reflection contrast spectra of Device 2 in Fig. 1b. The reflection contrast is defined as $\Delta R = (R - R_0)/R_0$, where $R_0$ is the background reflected intensity and $R$ is the reflected intensity from the sample. Clear moiré exciton peaks, labeled $MX_1$, $MX_2$ and $MX_3$, are observed in the spectra. The presence of these moiré excitons is a signature of a well-formed moiré lattice between the two layers[16–19]. Under finite doping, each moiré unit cell is sequentially filled with electrons[2,3], as indicated by the black arrows in the figure. At filling factor of $v = 1$ (i.e., one electron per moiré unit cell), an electron Mott insulator state forms due to onsite electron repulsion.

We also present a comparison of the moiré exciton intensities at filling factors of $v = 0$ and $v = 1$ in Fig. 1c. The data show that at $v = 1$, the optical response intensity of the $MX_2$ branch is comparable to that of the $MX_1$ branch under neutral condition. Given that both $MX_1$ and $MX_2$ branches can form polaritons under neutral conditions[11], this suggests the possibility of realizing a polariton state at the Mott insulating state ($v = 1$), termed a Mott insulator polariton. Conventionally, doping leads to a reduction of exciton oscillator strength in TMD monolayers[20]. However, within the $MoSe_2/WS_2$ system, Fig. 1b and 1c reveal a distinct behavior: $MX_2$ signal is enhanced under finite doping. The precise mechanism underlying this enhancement requires further investigation; it may reflect the unique exciton-charge interaction in the moiré superlattice[21–23]. Fig. 1d displays the peak intensities of the $MX_1$ and $MX_2$ branches, extracted from Fig. 1b, as a function of doping. It shows that $MX_1$ amplitude decreases continuously with increasing doping and disappears at around $v = 1$, whereas that of $MX_2$ initially increases, peaks at $v = 1$ and subsequently declines. Since the amplitude of $MX_3$ branch is negligible after doping (Fig. 1b), it is not considered in our study.

After characterizing the optical response of the bare moiré lattice, we proceeded to measure Device 1, where the moiré lattice was embedded within the cavity. The bare cavity mode was tuned by adjusting the PMMA thickness to match the $MX_1$ and $MX_2$ resonances. Angle-resolved reflection spectroscopy was employed to characterize the optical modes of the device. In Fig. 2a, the reflection spectra as a function of photon energy and angle are presented for the neutral moiré lattice ($v = 0$). Two anti-crossing features were observed at the $MX_1$ (1.600 eV) and $MX_2$ (1.647 eV) energies, indicating exciton-polariton formation for both moiré exciton branches, which is consistent with previous moiré polariton study[11]. From these measurements, the Rabi splitting energies for $MX_1$ and $MX_2$ polariton were extracted as 14.8 meV and 11.9 meV, denoted as $\Omega_1$ and $\Omega_2$, respectively (check Supplementary S7 for Rabi splitting extraction). This strong coupling is further evidenced by the well separated upper polariton (UP) and lower polariton (LP) branches in the spectrum at the angle of rabi splitting, indicated by vertical dashed lines in Fig. 2a (spectrum is shown in Supplementary Fig. S2).

Next, we investigated the effect of charge carriers on the polariton dispersion. The moiré lattice was doped by applying a positive gate voltage to the top silver gate while keeping the TMD layers grounded (Fig. 1a). Here, a positive gate voltage introduces electrons into the moiré lattice. Upon

finite doping, the oscillator strength of the $MX_1$ exciton decreases, while that of the $MX_2$ exciton increases (see Fig. 1b and 1d). Consequently, in the polariton dispersion, we observed a reduction in the $MX_1$ Rabi splitting and an enhancement of the $MX_2$ Rabi splitting, as shown in Fig. 2b, where the Rabi splitting for $MX_1$ and $MX_2$ changed to 11.2 meV and 17.3 meV, respectively. The electrical tunability of the Rabi splitting in the moiré exciton branches—both increasing and decreasing—demonstrates the versatility of the $MoSe_2/WS_2$ moiré system for the study of exciton-photon coupling. Note that in the single-gate geometry, doping and electric field vary simultaneously. To isolate the effect of the electric field on the Rabi splitting, we fabricated dual-gate Device 3. Its electric-field-dependent Rabi splitting (Supplementary Fig. S3) shows no discernable variation for either $MX_1$ or $MX_2$, indicating that contributions from the electric field are negligible.

When the doping level of the moiré lattice is further increased to the filling factor of $\nu = 1$, the $MX_1$ exciton fully loses its oscillator strength, while the $MX_2$ exciton reaches its maximum (Fig. 1c and 1d). At this point, we expect the Rabi splitting gap of $MX_1$ to close, accompanied by a maximized Rabi splitting for $MX_2$. This is indeed observed in Fig. 2c, where the $MX_2$ Rabi splitting reaches to $\Omega_2 = 21.9$ meV. Given that the moiré lattice is in a Mott insulator state at $\nu = 1$, combined with the large Rabi splitting, we conclude that a Mott insulator polariton has been realized in this moiré system at the $MX_2$ branch.

We also extracted the Rabi splitting for both $MX_1$ and $MX_2$ polariton as a function of charge density, as shown in Fig. 2d. The $MX_1$ polariton Rabi splitting decreases with doping and loses strong coupling around a filling factor of $\nu = 0.68$. In contrast, the $MX_2$ polariton Rabi splitting increases up to $\nu = 1$, after which further doping leads to its reduction (Supplementary Fig. S4 for $\nu = 2$ angle resolved reflection spectra). This trend fully aligns with the oscillator strength variations of the $MX_1$ and $MX_2$ excitons depicted in Fig. 1d. Future studies on the nonlinear interactions of this Mott insulator polariton could facilitate comparisons with other systems, such as bare moiré exciton polaritons[11,12], trion polaritons[13,24], Rydberg polaritons[25,26], and multilayer TMD polaritons[27], etc[28]. We note that the moiré twist angle, either 0° or 60°, does not appear to affect the formation of Mott insulator polaritons. This is evidenced in the Supplementary S5, where both 0° and 60° bare moiré devices exhibit enhanced $MX_2$ optical response at $\nu = 1$, indicating Mott insulator polariton can form in both twist angles.

The existence of Mott insulator polariton can be further evidenced by its magnetic field response. Typically, the response of an exciton polariton to magnetic fields is primarily governed by its excitonic constituent, a fact that has been consistently demonstrated in diverse platforms including 2D magnetic semiconductors[29,30], quantum wells[31], TMDs[32], etc. Fig. 3a and 3b present the angle-resolved reflection spectra of Device 1 at magnetic field B = -8 T and filling factor $\nu = 1$, measured with left ($\sigma^-$) and right ($\sigma^+$) circular polarization, respectively. The white dashed lines indicate their $MX_2$ resonance energies, corresponding to a ~4 meV splitting. The spectral difference of $MX_2$ between Fig. 3a and Fig. 3b indicates that the polaritons inherit valley polarization from the moiré excitons, whose valley Zeeman splitting induces the observed energy

shift[15]. We further extracted upper polariton energy versus magnetic field at $\nu = 1$ and at the angle of Rabi splitting, presented in Fig. 3c. The overall Zeeman energy shift between $\sigma^-$ and $\sigma^+$ polarizations at either 8 T or -8 T is approximately 4 meV, consistent with the bare moiré exciton splitting in Device 2 at $\nu = 1$, presented in Fig. 3d (more data in the Supplementary S6). Notably, both systems exhibit Zeeman shift saturation near $\pm 2$ T, where localized electron spins are fully polarized by external magnetic field. This parallel saturation behavior confirms the existence of Mott insulator polariton, that is, a polariton formed from a Mott insulator. We also extracted a polariton g-factor of 22.9 from Fig. 3c (check Supplementary S6). Compared to the g-factor of bare TMD monolayer excitons ($\sim 4$), trions ($\sim 20$) and their respective polaritons[32,33], the large g-factor of the Mott insulator polariton could also be advantageous for polariton applications requiring time-reversal symmetry breaking, such as topological photonics[34]. We also want to mention that in this work, we focused only on the integer filling factor $\nu = 1$, as the oscillator strength of fractional fillings states is too weak to be detected in our moiré exciton reflection measurements. This contrasts with techniques such as 2s sensing[35], which can resolve these states. Future improvements in sample quality may enhance the oscillator strength of fractional states, enabling their coupling to the cavity to form generalized Wigner crystal polaritons. In such a phase, repulsion between neighboring moiré sites would break the lattice translation symmetry, potentially leading to polariton interaction energies distinct from those in the Mott insulator polariton. Furthermore, the smaller energy gaps of these fractional states could, upon strong coupling with the cavity, be modified to potentially induce polariton-mediated correlation phase transitions[36].

In conclusion, we have demonstrated a Mott insulator polariton realized through a silver gated structure. Its existence is confirmed by doping-dependent angle-resolved reflection measurements, which reveal a maximum Rabi splitting of the $MX_2$ moiré exciton at a moiré lattice filling of $\nu = 1$. The magnetic Zeeman energy shift of the Mott insulator polariton follows a trend similar to that of bare moiré excitons. Our results highlight the doping and magnetic tunability of moiré lattice polaritons. Future investigations should focus on the polariton interaction strength at filling $\nu = 1$ to elucidate the many-body nonlinear interactions among electrons, excitons, and photons in this system. Such studies could further advance the potential applications of these polaritons in quantum technologies.

## Contributions

X.G., H.G. fabricated the devices and performed the measurements. X.G. analyzed the data. K.W. and T.T. grew the bulk hBN crystals. J.G., Z.C. designed the scientific objectives, oversaw the project and cowrote the manuscript. All authors discussed the results and commented on the manuscript.

## Supporting Information

Methods of moiré structure and cavity sample fabrication, polariton spectra at $\nu = 0$, dual-gate device data, angle resolved reflection spectra at $\nu = 2$, comparison of 0° and 60° twist devices, more magnetic data of Device 1 and Device 2, and description of polariton dispersion.


## Acknowledgments

The work is supported by the National Key Research and Development Program of China (2023YFA1407100), the National Natural Science Foundation of China (12374068). K.W. and T.T. acknowledge support from the JSPS KAKENHI (21H05233 and 23H02052), the CREST (JPMJCR24A5), JST and World Premier International Research Center Initiative (WPI), MEXT, Japan. Part of the sample fabrication was performed at Fudan Nano-fabrication Laboratory. J.G. also acknowledges the use of the magnetic field setup, a facility supported by the University Nano Information Science Innovation Support Center Project of the Ministry of Education of China, which was provided by the Frontier Institute of Chip and System and the Nano Institute of Fudan University.


## References


(1) Mak, K. F.; & Shan, J. Semiconductor moiré materials. *Nat. Nanotechnol.* **2022**, *17* (7), 686–695.

(2) Regan, E. C.; Wang, D.; Jin, C.; Bakti Utama, M. I.; Gao, B.; Wei, X.; Zhao, S.; Zhao, W.; Zhang, Z.; Yumigeta, K.; Blei, M.; Carlström, J. D.; Watanabe, K.; Taniguchi, T.; Tongay, S.; Crommie, M.; Zettl, A.; & Wang, F. Mott and generalized Wigner crystal states in $WSe_2/WS_2$ moiré superlattices. *Nature* **2020**, *579* (7799), 359–363.

(3) Tang, Y.; Li, L.; Li, T.; Xu, Y.; Liu, S.; Barmak, K.; Watanabe, K.; Taniguchi, T.; MacDonald, A. H.; Shan, J.; & Mak, K. F. Simulation of Hubbard model physics in $WSe_2/WS_2$ moiré superlattices. *Nature* **2020**, *579* (7799), 353–358.

(4) Xia, Y.; Han, Z.; Watanabe, K.; Taniguchi, T.; Shan, J.; & Mak, K. F. Superconductivity in twisted bilayer $WSe_2$. *Nature* **2025**, *637* (8047), 833–838.

(5) Guo, Y.; Pack, J.; Swann, J.; Holtzman, L.; Cothrine, M.; Watanabe, K.; Taniguchi, T.; Mandrus, D. G.; Barmak, K.; Hone, J.; Millis, A. J.; Pasupathy, A.; & Dean, C. R. Superconductivity in 5.0° twisted bilayer $WSe_2$. *Nature* **2025**, *637* (8047), 839–845.

(6) Li, H.; Li, S.; Regan, E. C.; Wang, D.; Zhao, W.; Kahn, S.; Yumigeta, K.; Blei, M.; Taniguchi, T.; Watanabe, K.; Tongay, S.; Zettl, A.; Crommie, M. F.; & Wang, F. Imaging two-dimensional generalized Wigner crystals. *Nature* **2021**, *597* (7878), 650–654.

(7) Li, H.; Xiang, Z.; Reddy, A. P.; Devakul, T.; Sailus, R.; Banerjee, R.; Taniguchi, T.; Watanabe, K.; Tongay, S.; Zettl, A.; Fu, L.; Crommie, M. F.; & Wang, F. Wigner molecular crystals from multielectron moiré artificial atoms. *Science* **2024**, *385* (6704), 86–91.

(8) Deng, H.; Haug, H.; & Yamamoto, Y. Exciton-polariton Bose-Einstein condensation. *Rev. Mod. Phys.* **2010**, *82* (2), 1489–1537.

(9) Sanvitto, D.; & Kéna-Cohen, S. The road towards polaritonic devices. *Nature Mater.* **2016**, *15* (10), 1061–1073.

(10) Ghosh, S.; & Liew, T. C. H. Quantum computing with exciton-polariton condensates. *npj Quantum Inf* **2020**, *6* (1), 16.

(11) Zhang, L.; Wu, F.; Hou, S.; Zhang, Z.; Chou, Y.-H.; Watanabe, K.; Taniguchi, T.; Forrest, S. R.; & Deng, H. Van der Waals heterostructure polaritons with moiré-induced nonlinearity. *Nature* **2021**, *591* (7848), 61–65.

(12) Fitzgerald, J. M.; Thompson, J. J. P.; & Malic, E. Twist Angle Tuning of Moiré Exciton Polaritons in van der Waals Heterostructures. *Nano Lett.* **2022**, *22* (11), 4468–4474.

(13) Sidler, M.; Back, P.; Cotlet, O.; Srivastava, A.; Fink, T.; Kroner, M.; Demler, E.; & Imamoglu, A. Fermi polaron-polaritons in charge-tunable atomically thin semiconductors. *Nature Phys* **2017**, *13* (3), 255–261.

(14) Gu, J.; Chakraborty, B.; Khatoniar, M.; & Menon, V. M. A room-temperature polariton light-emitting diode based on monolayer WS2. *Nat. Nanotech.* **2019**, *14* (11), 1024–1028.

(15) Scherzer, J.; Lackner, L.; Han, B.; Polovnikov, B.; Husel, L.; Göser, J.; Li, Z.; Drawer, J.-C.; Esmann, M.; Bennenhei, C.; Eilenberger, F.; Watanabe, K.; Taniguchi, T.; Baimuratov, A. S.; Schneider, C.; & Högele, A. Correlated magnetism of moiré exciton-polaritons on a triangular electron-spin lattice. *arXiv* **2024**, DOI: 10.48550/arXiv.2405.12698.

(16) Jin, C.; Regan, E. C.; Yan, A.; Iqbal Bakti Utama, M.; Wang, D.; Zhao, S.; Qin, Y.; Yang, S.; Zheng, Z.; Shi, S.; Watanabe, K.; Taniguchi, T.; Tongay, S.; Zettl, A.; & Wang, F. Observation of moiré excitons in WSe2/WS2 heterostructure superlattices. *Nature* **2019**, *567* (7746), 76–80.

(17) Alexeev, E. M.; Ruiz-Tijerina, D. A.; Danovich, M.; Hamer, M. J.; Terry, D. J.; Nayak, P. K.; Ahn, S.; Pak, S.; Lee, J.; Sohn, J. I.; Molas, M. R.; Koperski, M.; Watanabe, K.; Taniguchi, T.; Novoselov, K. S.; Gorbachev, R. V.; Shin, H. S.; Fal'ko, V. I.; & Tartakovskii, A. I. Resonantly hybridized excitons in moiré superlattices in van der Waals heterostructures. *Nature* **2019**, *567* (7746), 81–86.

(18) Tang, Y.; Gu, J.; Liu, S.; Watanabe, K.; Taniguchi, T.; Hone, J. C.; Mak, K. F.; & Shan, J. Dielectric catastrophe at the Wigner-Mott transition in a moiré superlattice. *Nat Commun* **2022**, *13* (1), 4271.

(19) Gu, J.; Zhu, J.; Knuppel, P.; Watanabe, K.; Taniguchi, T.; Shan, J.; & Mak, K. F. Remote imprinting of moiré lattices. *Nat. Mater.* **2024**, *23* (2), 219–223.

(20) Mak, K. F.; He, K.; Lee, C.; Lee, G. H.; Hone, J.; Heinz, T. F.; & Shan, J. Tightly bound trions in monolayer MoS2. *Nature Mater* **2013**, *12* (3), 207–211.

(21) Naik, M. H.; Regan, E. C.; Zhang, Z.; Chan, Y.-H.; Li, Z.; Wang, D.; Yoon, Y.; Ong, C. S.; Zhao, W.; Zhao, S.; Utama, M. I. B.; Gao, B.; Wei, X.; Sayyad, M.; Yumigeta, K.; Watanabe, K.; Taniguchi, T.; Tongay, S.; Jornada, F. H. da; Wang, F.; & Louie, S. G. Intralayer charge-transfer moiré excitons in van der Waals superlattices. *Nature* **2022**, *609* (7925), 52–57.

(22) Ciorciaro, L.; Smoleński, T.; Morera, I.; Kiper, N.; Hiestand, S.; Kroner, M.; Zhang, Y.; Watanabe, K.; Taniguchi, T.; Demler, E.; & İmamoğlu, A. Kinetic magnetism in triangular moiré materials. *Nature* **2023**, *623* (7987), 509–513.

(23) Polovnikov, B.; Scherzer, J.; Misra, S.; Huang, X.; Mohl, C.; Li, Z.; Göser, J.; Förste, J.; Bilgin, I.; Watanabe, K.; Taniguchi, T.; Högele, A.; & Baimuratov, A. S. Field-Induced Hybridization of Moiré Excitons in $MoSe_2/WS_2$ Heterobilayers. *Phys. Rev. Lett.* **2024**, *132* (7), 076902.

(24) Emmanuele, R. P. A.; Sich, M.; Kyriienko, O.; Shahnazaryan, V.; Withers, F.; Catanzaro, A.; Walker, P. M.; Benimetskiy, F. A.; Skolnick, M. S.; Tartakovskii, A. I.; Shelykh, I. A.; & Krizhanovskii, D. N. Highly nonlinear trion-polaritons in a monolayer semiconductor. *Nat Commun* **2020**, *11* (1), 3589.

(25) Gu, J.; Walther, V.; Waldecker, L.; Rhodes, D.; Raja, A.; Hone, J. C.; Heinz, T. F.; Kéna-Cohen, S.; Pohl, T.; & Menon, V. M. Enhanced nonlinear interaction of polaritons via excitonic Rydberg states in monolayer WSe2. *Nat Commun* **2021**, *12* (1), 2269.

(26) Bao, W.; Liu, X.; Xue, F.; Zheng, F.; Tao, R.; Wang, S.; Xia, Y.; Zhao, M.; Kim, J.; Yang, S.; Li, Q.; Wang, Y.; Wang, Y.; Wang, L.-W.; MacDonald, A. H.; & Zhang, X. Observation of Rydberg exciton polaritons and their condensate in a perovskite cavity. *Proceedings of the National Academy of Sciences* **2019**, *116* (41), 20274–20279.

(27) Zhao, J.; Fieramosca, A.; Dini, K.; Bao, R.; Du, W.; Su, R.; Luo, Y.; Zhao, W.; Sanvitto, D.; Liew, T. C. H.; & Xiong, Q. Exciton polariton interactions in Van der Waals superlattices at room temperature. *Nat Commun* **2023**, *14* (1), 1512.

(28) Luo, Y.; Zhao, J.; Fieramosca, A.; Guo, Q.; Kang, H.; Liu, X.; Liew, T. C. H.; Sanvitto, D.; An, Z.; Ghosh, S.; Wang, Z.; Xu, H.; & Xiong, Q. Strong light-matter coupling in van der Waals materials. *Light Sci Appl* **2024**, *13* (1), 203.

(29) Dirnberger, F.; Quan, J.; Bushati, R.; Diederich, G. M.; Florian, M.; Klein, J.; Mosina, K.; Sofer, Z.; Xu, X.; Kamra, A.; García-Vidal, F. J.; Alù, A.; & Menon, V. M. Magneto-optics in a van der Waals magnet tuned by self-hybridized polaritons. *Nature* **2023**, *620* (7974), 533–537.

(30) Li, C.; Shen, C.; Jiang, N.; Tang, K. K.; Liu, X.; Guo, J.; Liang, Y.; Song, J.; Deng, X.; & Zhang, Q. 2D CrSBr Enables Magnetically Controllable Exciton-Polaritons in an Open Cavity. *Advanced Functional Materials* **2024**, *34* (51), 2411589.

(31) Larionov, A. V. Polarized Nonequilibrium Bose-Einstein Condensates of Spinor Exciton Polaritons in a Magnetic Field. *Phys. Rev. Lett.* **2010**, *105* (25),

(32) Lyons, T. P.; Gillard, D. J.; Leblanc, C.; Puebla, J.; Solnyshkov, D. D.; Klompmaker, L.; Akimov, I. A.; Louca, C.; Muduli, P.; Genco, A.; Bayer, M.; Otani, Y.; Malpuech, G.; & Tartakovskii, A. I. Giant effective Zeeman splitting in a monolayer semiconductor realized by spin-selective strong light–matter coupling. *Nat. Photon.* **2022**, *16* (9), 632–636.

(33) Förste, J.; Tepliakov, N. V.; Kruchinin, S. Y.; Lindlau, J.; Funk, V.; Förg, M.; Watanabe, K.; Taniguchi, T.; Baimuratov, A. S.; & Högele, A. Exciton g-factors in monolayer and bilayer WSe2 from experiment and theory. *Nat Commun* **2020**, *11* (1), 4539.

(34) Klembt, S.; Harder, T. H.; Egorov, O. A.; Winkler, K.; Ge, R.; Bandres, M. A.; Emmerling, M.; Worschech, L.; Liew, T. C. H.; Segev, M.; Schneider, C.; & Höfling, S. Exciton-polariton topological insulator. *Nature* **2018**, *562* (7728), 552–556.

(35) Xu, Y.; Liu, S.; Rhodes, D. A.; Watanabe, K.; Taniguchi, T.; Hone, J.; Elser, V.; Mak, K. F.; & Shan, J. Correlated insulating states at fractional fillings of moiré superlattices. *Nature* **2020**, *587* (7833), 214–218.

(36) Sun, K.; & Deng, H. Polariton-induced unconventional superconductivity and emergent SU(2) symmetry in moiré flat bands. *Materials Today Quantum* **2025**, *6* 100039.

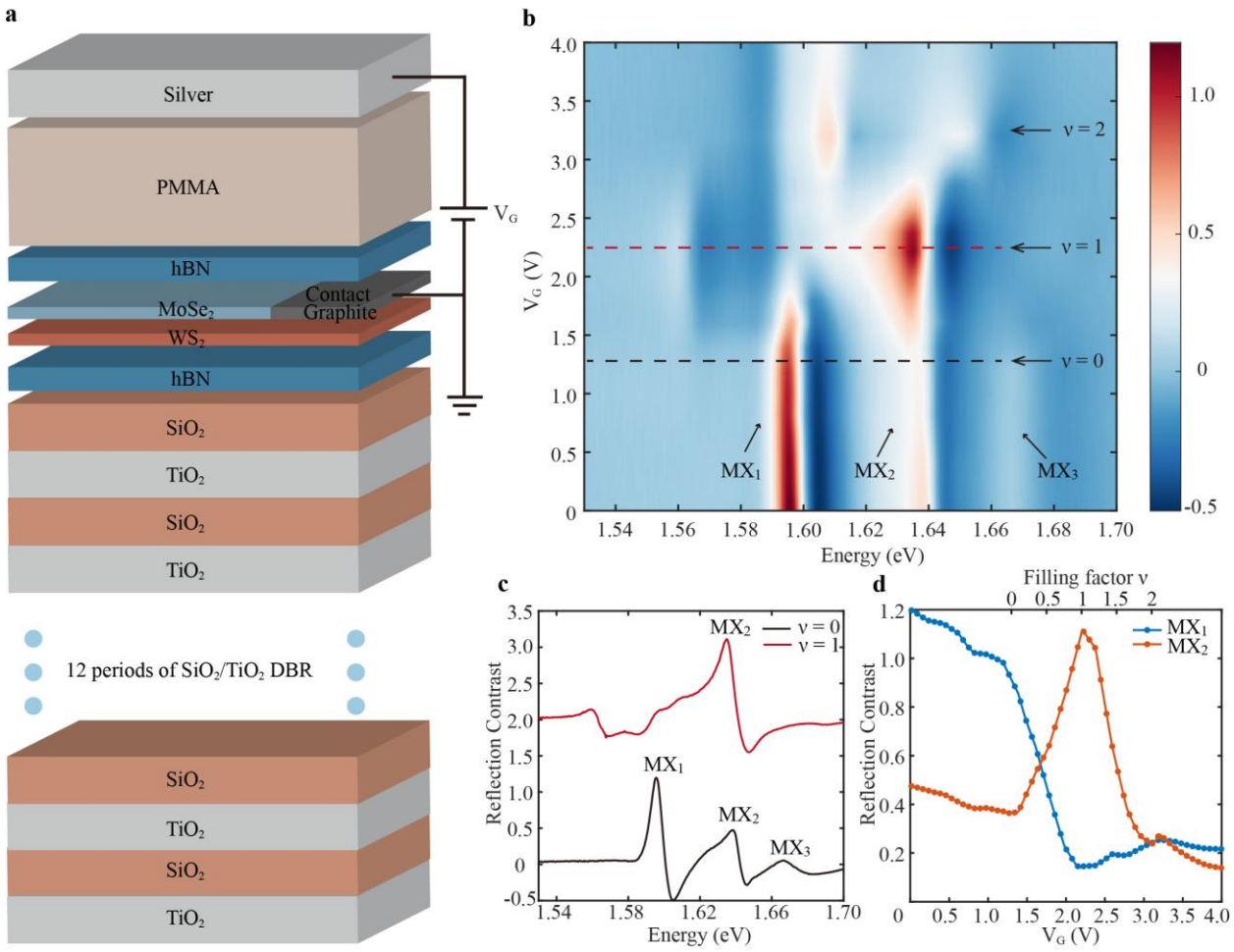



Figure 1. Optical Characterization of $MoSe_2/WS_2$ Heterostructure. (a) Schematic of Mott insulator polariton device (Device 1). (b) Gate dependent reflection contrast spectra of the bare moiré structure (Device 2). $\nu = 0$ corresponds to the charge neutrality point; below this voltage, the structure is charge neutral. The resonance at $\nu = 1$ and Energy $\approx 1.56$ eV is attributed to the attractive polaron of $MX_1$. (c) Reflection contrast spectra at $\nu = 0$ (black) and $\nu = 1$ (red), corresponding to the dashed lines in (b). The $\nu = 1$ spectrum is vertically offset for clarity. (d) Gate-voltage dependence of the reflection contrast amplitude for $MX_1$ (blue) and $MX_2$ (orange) in (b). The $MX_1$ amplitude was determined from the maximum intensity within the energy range 1.59 – 1.60 eV, while $MX_2$ was extracted between 1.63 eV and 1.64 eV.

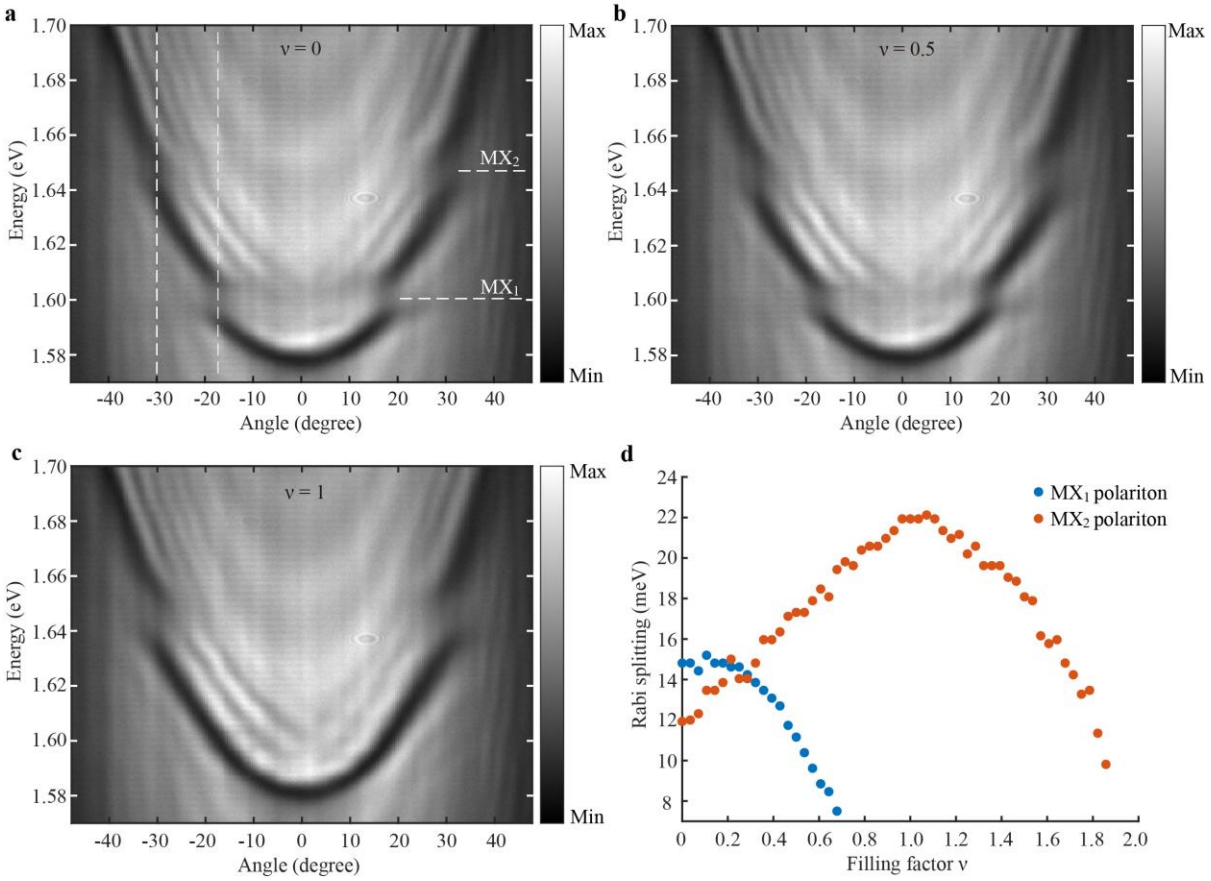



Figure 2. Mott insulator polariton. (a–c) Angle-resolved reflection spectra of Device 1 at filling factors $\nu = 0$ (a), $\nu = 0.5$ (b), and $\nu = 1$ (c). Detailed optical measurements of the setup are provided in Supplementary S1. In (a), the angles of Rabi splitting (vertical dashed lines) and the $MX_1$, $MX_2$ resonance energies (horizontal dashed lines) are indicated. Note that here the $MX_1$ and $MX_2$ energies differ from those of the bare moiré exciton in Device 2 (Fig. 1b) due to device-to-device variation. (d) Rabi splitting energy associated with $MX_1$ (blue) and $MX_2$ (orange) polaritons as a function of filling factor. The Mott insulator polariton emerges in the $MX_2$ branch at $\nu = 1$.

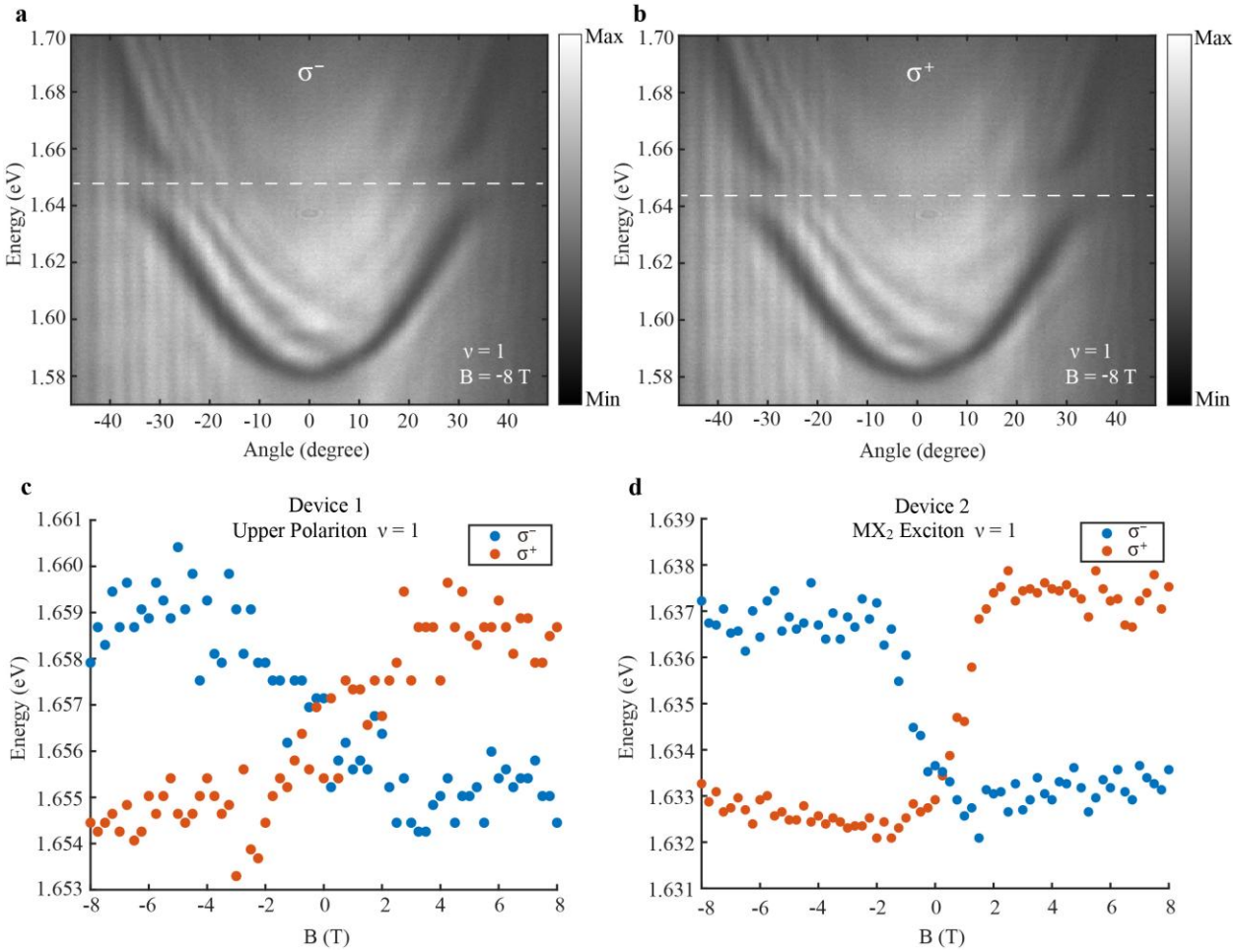



Figure 3. Magnetic field response of Mott insulator polariton. (a), (b) Angle-resolved reflection spectra of Device 1 at B = -8 T and $\nu = 1$, under $\sigma^-$ (a) and $\sigma^+$ (b) polarization, respectively. The energies of the $MX_2$ feature are indicated by white dashed lines in both panels. They were determined from the polariton dispersion by measuring the minimum energy difference between the upper and lower polariton branches (see Supplementary S7). (c), (d) At $\nu = 1$, the magnetic field dependence of the upper polariton energy (c) at the angle of Rabi splitting in Device 1 and $MX_2$ energy (d) in Device 2, measured under $\sigma^-$ (blue) and $\sigma^+$ (orange) polarization.